

**INVESTIGATIONS ON SILVER-COPPER  
NANOPASTE AS DIE-ATTACH MATERIAL FOR  
HIGH TEMPERATURE APPLICATIONS**

**TAN KIM SEAH**

**UNIVERSITI SAINS MALAYSIA**

**2015**

# **INVESTIGATIONS ON SILVER-COPPER NANOPASTE AS DIE-ATTACH MATERIAL FOR HIGH TEMPERATURE APPLICATIONS**

**by**

**TAN KIM SEAH**

**Thesis submitted in fulfillment of the requirements**

**for the Degree of**

**Doctor of Philosophy**

**JANUARY 2015**

## PENGISYTIHARAN / *DECLARATION*

Saya isytiharkan bahawa kandungan yang dibentangkan di dalam tesis ini adalah hasil kerja saya sendiri dan telah dijalankan di Universiti Sains Malaysia kecuali dimaklumkan sebaliknya.

*I declare that the contents presented in this thesis are my own work which was done at Universiti Sains Malaysia unless stated otherwise. The thesis has not been previously submitted for any other degree.*

---

Tandatangan Calon /

*Signature of Candidate*

Nama Calon / *Name of Candidate*

**TAN KIM SEAH**

Tarikh / *Date*

**JANUARY 2015**

---

Tandatangan Penyelia /

*Signature of Supervisor*

Nama Penyelia & Cop Rasmi /

*Name of Supervisor & Official Stamp*

**PROFESSOR IR. DR.**

**CHEONG KUAN YEW**

Tarikh / *Date*

**JANUARY 2015**

## **ACKNOWLEDGEMENTS**

I would like to take this opportunity to express my heartiest gratitude to the following people for their invaluable help rendered during my Ph.D journey.

First and foremost, I would like to express my sincere thanks to my supervisor, Professor Ir. Dr. Cheong Kuan Yew, for his invaluable advice, support, and patience throughout the research studies. His guidance, advises encouragement, and constructive suggestions enabled me to handle the project well.

I also want to express my gratitude to the Dean, Professor Dr. Hanafi Ismail and all academic and administrative staffs of the School of Materials and Mineral Resources Engineering for their continual assistance and supports.

I would like to express my sincere thanks to Mr. Mohd Suhaimi Sulong, Mdm. Fong Lee Lee, Mr. Mohd Azam, Mr. Mokhtar and all technical staffs, for their patience in guiding me during the study. Also, I would like to thank to all technical staffs from Nano-optoelectronic Research (N.O.R) lab of the School of Physics. This research would be nothing without the enthusiasm and assistance from them.

I am deeply indebted to my colleagues-cum-friends associated in Electronic Materials Research Group, especially Khor Li Qian, Quah Hock Jin, Lim Way

Foong, Vemal Raja Manikam, Mohammad Saleh Gorji, Tan Pi Lin and Lim Zhe Xi, for their invaluable supports and suggestions throughout the project.

A great appreciation is dedicated to my loved family members, especially my parents and brothers, for their love, unfailing encouragement and support.

Last but not least, I would like to acknowledge the financial assistance provided by Universiti Sains Malaysia via Research University Postgraduate Research Grant Scheme (USM-RU-PRGS), and Ministry of Education Malaysia via MyPhD scholarship program.

## TABLE OF CONTENTS

	Page
ACKNOWLEDGEMENTS	ii
TABLE OF CONTENTS	iv
LIST OF TABLES	x
LIST OF FIGURES	xii
LIST OF ABBREVIATIONS	xix
LIST OF SYMBOLS	xxi
LIST OF PUBLICATIONS	xxiii
ABSTRAK	xxv
ABSTRACT	xxvii
 CHAPTER 1: INTRODUCTION	
1.1 Theoretical Background	1
1.2 Problem Statement	3
1.3 Research Objectives	9
1.4 Scope of Study	10
1.5 Thesis Outline	11
 CHAPTER 2: LITERATURE REVIEW	
2.1 Introduction	13
2.2 Definition of High-Temperature for Electronic Device	14
2.3 Evolution of Semiconductor in Electronic Device	14
2.3.1 Demands of High-Temperature Electronic Device	17
2.4 An Overview of Electronic Packaging	22

2.5	Materials for Level-One Electronic Packaging	23
2.5.1	Requirements for High-Temperature Die-Attach Materials	25
2.6	Classification of Die-Attach Materials	32
2.6.1	Conductive Adhesive	32
2.6.2	Conductive Glass	35
2.6.3	Solder Alloy	38
2.6.3.1	Tin Based Solder Alloy (Lead-Bearing and Lead-Free)	39
2.6.3.2	Gold Based Solder Alloy	44
2.6.3.3	Bismuth Based Solder Alloy	49
2.6.3.4	Zinc Based Solder Alloy	53
2.6.4	Metal Film	60
2.6.5	Metal Paste	62
2.7	Factors Affecting Properties of Die-Attach Materials	73
2.7.1	Interfaces	74
2.7.2	Defects	77
2.8	Ag-Cu system	79
2.9	Nanoparticles	82
2.10	Sintering of Nanoparticles	84
2.11	Organic Additives for Nanopaste Formulation	88
2.12	Summary	89

## CHAPTER 3: MATERIALS AND METHODOLOGY

3.1	Introduction	91
3.2	Materials	94
3.2.1	Materials for Ag-Cu Nanopaste Formulation	94
3.2.2	Substrate Materials	95
3.2.3	Materials for Substrate Cleaning	95
3.2.4	SiC Die	96
3.2.5	Materials for SiC Die Cleaning	96
3.2.6	Materials for SiC Die and Substrate Metallization	96
3.3	Experimental Procedures	97
3.3.1	Substrate Cleaning Process	97
3.3.2	Formulation of Ag-Cu Nanopaste	98
3.3.3	Stencil Printing of the Ag-Cu Nanopaste	100
3.3.4	Sintering of the Ag-Cu Nanopaste	101
3.3.5	SiC Die Cleaning Process	103
3.3.6	Metallization Coating for SiC Die and Cu Substrate	105
3.3.7	Thermal Aging Test on Sintered Nanopaste	106
3.3.8	Cross-Section Failure Analysis	107
3.4	Characterization Techniques	108
3.4.1	Physical Characterization	108
3.4.1.1	Field Emission Scanning Electron Microscopy (FE-SEM)	108
3.4.1.2	Energy-Filtered Transmission Electron Microscopy (EF-TEM)	108
3.4.1.3	Atomic Force Microscopy (AFM)	109



3.4.1.4	X-Ray Diffraction (XRD)	109
3.4.1.5	Rheological Study	109
3.4.1.6	Density and Porosity	110
3.4.1.7	Carbon-Hydrogen-Nitrogen-Sulfur (CHNS)	111
	Elemental Analysis	
3.4.2	Electrical Characterization	111
3.4.3	Thermal Characterization	112
3.4.3.1	Differential Scanning Calorimetry (DSC)	112
3.4.3.2	Thermogravimetric Analysis (TGA)	113
3.4.3.3	Thermomechanical Analysis (TMA)	113
3.4.3.4	Nanoflash Laser	114
3.4.4	Mechanical Characterization	115
3.4.4.1	Nanoindentation	115
3.4.4.2	Lap Shear Test	115

## CHAPTER 4: RESULTS AND DISCUSSION

4.1	Introduction	117
4.2	Formulation of Ag-Cu Nanopaste	118
4.2.1	Determination of the Characteristics of Ag and Cu Nanoparticles	118
4.2.2	Determination of the Characteristics of Organic Additives	122
4.2.3	Rheological Properties of Ag-Cu Nanopaste With Various Nanoparticle Loadings	124
4.3	Determination of Sintering Temperature for Ag-Cu Nanopaste	127

4.3.1	Physical and Electrical Characteristics	127
4.4	Determination of Sintering Environment for Ag-Cu Nanopaste	132
4.4.1	Physical and Electrical Characteristics	132
4.5	Investigation of Physical and Electrical Characteristics of Ag-Cu Nanopaste With Various Cu Loadings	136
4.5.1	Rheological Properties	137
4.5.2	XRD Analysis	140
4.5.3	Density and Porosity Analysis	143
4.5.4	Surface Morphology Analysis	144
4.5.5	Electrical Conductivity Measurements	149
4.5.6	Summary	152
4.6	Investigation of Thermal Characteristics of Ag-Cu Nanopaste With Various Cu Loadings	153
4.6.1	Melting Point and Safety Operating Temperature	153
4.6.2	Specific Heat, Thermal Diffusivity and Thermal Conductivity	157
4.6.3	Thermal Expansion	165
4.6.4	Summary	176
4.7	Investigation of Mechanical Characteristics of Ag-Cu Nanopaste With Various Cu Loadings	176
4.7.1	Hardness, Young's Modulus and Stiffness	177
4.7.2	Bonding Attributes of Ag-Cu Nanopaste	184
4.7.3	Thermal Shock Resistance	187
4.7.4	Summary	189
4.8	Investigation of the Bonding Attributes on Different Metallizations	193

4.8.1	Effect of Metallization on Bonding Attributes	193
4.9	Application of Ag-Cu Nanopaste and Its Adhesion Performance After Thermal Aging	198
CHAPTER 5: CONCLUSION AND FUTURE RECOMMENDATIONS		
5.1	Conclusion	204
5.2	Recommendations For Future Work	206
REFERENCES		207
APPENDICES		226

## LIST OF TABLES

		Page
Table 1.1	Benchmark requirements of various die-attach properties for SiC device	2
Table 1.2	Properties of bulk Ag, Cu, Au and Al	8
Table 2.1	A comparison of semiconductor properties between Si and SiC	16
Table 2.2	Automotive maximum operating temperatures	20
Table 2.3	A summary of various gases sensed by SiC-based gas sensors	24
Table 2.4	Summary properties of conductive adhesive	35
Table 2.5	Summary properties of conductive glass	37
Table 2.6	Eutectic temperature of various Sn based binary solder alloys	41
Table 2.7	Melting temperature of various Pb-free Sn based ternary and quaternary solder alloys and composites	42
Table 2.8	Summary properties of Au-20Sn, Au-12Ge and Au-3Si eutectic solder alloys	48
Table 2.9	Summary properties of various Bi based solder alloys	49
Table 2.10	Solidus and liquidus temperatures of various Zn based solder alloys	53
Table 2.11	Summary properties of various Zn based solder alloys	59
Table 2.12	Summary properties of various metal pastes	71
Table 2.13	Selected characteristics of Ag and Cu	82
Table 2.14	Reported organic additives in nanopaste formulation	89
Table 3.1	Raw materials used for Ag-Cu nanopaste formulation	94

Table 3.2	List of chemicals for substrate cleaning	96
Table 3.3	List of chemicals for SiC die cleaning	96
Table 3.4	Materials used for metallization	97
Table 3.5	Formula of Ag-Cu nanopaste with various organic additive contents	99
Table 3.6	Step by step cleaning process for SiC die	103
Table 4.1	Weight ratio of Ag and Cu nanoparticles for pure Ag nanopaste, pure Cu nanopaste and Ag-Cu nanopaste	137
Table 4.2	Electrical conductivity of Ag-Cu nanopaste versus typical die-attach systems	152
Table 4.3	Thermal conductivity, CTE and performance index for various die-attach systems	163
Table 4.4	The CTE difference between typical high-temperature die-attach systems and electronic packaging components	171
Table 4.5	Thermal conductivity, CTE and performance index for various dies and substrates for high-temperature applications	175
Table 4.6	Hardness, Young's modulus and porosity of sintered pure Ag, pure Cu and Ag-Cu nanopastes in against bulk Ag and Cu	183
Table 4.7	Hardness and Young's modulus of sintered Ag-Cu nanopaste in against typical die-attach systems	185
Table 4.8	Thermal conductivity, CTE, Young's modulus, fracture strength and thermal shock resistance for various die-attach systems, dies and substrates	190
Table 5.1	Summary properties of sintered Ag-20Cu nanopaste	206

## LIST OF FIGURES

		Page
Figure 2.1	Hierarchy of electronic packaging	23
Figure 2.2	Schematic drawing of (a) ICA and (b) ACA	33
Figure 2.3	Firing profile for conductive glass	36
Figure 2.4	Melting temperature of Sn-Pb solder alloy with increasing of Pb loading	40
Figure 2.5	Cross-sectional SEM image of Au-20Sn solder reflowed at 280 °C for (a) 10 s and (b) 60 s. The lighter region is Au <sub>5</sub> Sn and the darker region is AuSn	45
Figure 2.6	SEM micrograph of reflowed (a) Au-12Ge and (b) Au-3Si solder alloys	47
Figure 2.7	Microstructure of reflowed Bi-2.5Ag and Bi-11Ag solder alloys	50
Figure 2.8	(a) Shear strength of Bi-Ag solder alloy with various Ag loadings; (b) a comparison of shear strength of Bi-Ag solder alloy with and without minor addition of Ce	51
Figure 2.9	Electrical resistivity of Bi-2.6Ag-0.1Cu-(0-2)Sb solder alloy	52
Figure 2.10	SEM micrographs of Zn-Sn solder alloy with (a) 40 wt%, (b) 30 wt% and (c) 20 wt% of Sn loading	55
Figure 2.11	Shear strength and thermal conductivity of Zn-(20-40)Sn in against of Au-20Sn and Pb-5Sn solder alloys	56
Figure 2.12	Shear strength of Zn-6Al-5Ge solder alloy at different reflow temperatures in against of Pb-5Sn solder alloy	57
Figure 2.13	Shear strength of Zn-4Al-3Mg-3Ga solder alloy at different reflow temperatures in against of Pb-5Sn solder alloy	58
Figure 2.14	Pull strength of Au-In and Ag-In systems fir before and after annealing processes	61

Figure 2.15	Formulation steps of Ag nanopaste	65
Figure 2.16	(a) Shear strength of Cu nanopaste that sintered at various temperatures and pressures; (b) shear strength of Cu nanopaste that sintered at various temperatures and environments	67
Figure 2.17	Bonding shear strength as a function of sintering temperature. Dashed line represents Ag micropaste and solid line represents Ag hybrid paste	69
Figure 2.18	Shear strength, porosity and thermal conductivity of Ag hybrid paste that sintered under different combinations of dwell time and pressure	70
Figure 2.19	Schematic diagram of a semiconductor die attached on a substrate using die-attach material	74
Figure 2.20	(a) Intermetallic formation of Sn solder alloy; (b) grooving of Bi-Ag solder alloy; and (c) atomic diffusion of Ag metal paste	75
Figure 2.21	The silver-copper phase diagram	80
Figure 2.22	Melting temperature for Ag and Cu as a function of particle size	83
Figure 2.23	Atomic transport paths during sintering	85
Figure 2.24	Illustration of the sintering stages	86
Figure 3.1	An overview of the research methodology	92
Figure 3.2	An overview on characterization techniques used in this work	93
Figure 3.3	AlN DBC substrate for die-attach	95
Figure 3.4	Formulation process flow for Ag-Cu nanopaste	100
Figure 3.5	Schematic cross sectional view of Ag-Cu nanopaste stencil printed on either pre-cleaned Cu substrate or pre-clean soda lime glass substrate	101

Figure 3.6	The experimental setup for sintering Ag-Cu nanopaste in open air ambient	102
Figure 3.7	The experimental setup for sintering Ag-Cu nanopaste with flow of either nitrogen or argon gas	103
Figure 3.8	Schematic cross sectional view of SiC die attached on either bare Cu substrate or AlN DBC substrate using Ag-Cu nanopaste	107
Figure 3.9	(a) Schematic top view configuration of a single lap shear joint specimen, and (b) setup of the lap shear test	116
Figure 4.1	XRD diffractogram for as-received commercial Ag and Cu nanoparticles	119
Figure 4.2	Particle size distribution for as-received commercial Ag and Cu nanoparticles	119
Figure 4.3	DSC thermograph for as-received commercial Ag and Cu nanoparticles	120
Figure 4.4	TGA thermograph for as-received commercial Ag and Cu nanoparticles	121
Figure 4.5	TEM image of Ag and Cu nanoparticles that covered by a thin layer of ethylene glycol	123
Figure 4.6	TGA thermogram for various organic additives used in nanopaste	124
Figure 4.7	Flow curve for Ag-20Cu nanopaste with various loadings of nanoparticle	125
Figure 4.8	The appearance of Ag-20Cu nanopaste with various loadings of nanoparticle; (a) $\leq 87$ wt%, (b) 88 wt% and (c) 89 wt%	126
Figure 4.9	FE-SEM micrographs of Ag-20Cu nanopaste sintered at open air and various sintering temperatures	128
Figure 4.10	XRD diffractogram of Ag-20Cu nanopaste sintered at open air and various sintering temperatures	130



Figure 4.11	Electrical conductivity of Ag-20Cu nanopaste sintered at open air and various sintering temperatures	131
Figure 4.12	XRD diffractogram of Ag-20Cu nanopaste sintered with various sintering environments and temperature of 380 °C	133
Figure 4.13	Carbon content of Ag-20Cu nanopaste sintered with various sintering environments and temperature of 380 °C	134
Figure 4.14	FE-SEM micrographs of Ag-20Cu nanopaste that sintered in (a) open air, (b) nitrogen and (c) argon ambient	135
Figure 4.15	Electrical conductivity of Ag-20Cu nanopaste sintered with various sintering environments and temperature of 380 °C.	136
Figure 4.16	(a) Schematic of organic binder that linked-up the nanoparticles with surfactant coating, (b) typical appearance of Ag-Cu nanopaste with desired stencil printable quality	138
Figure 4.17	Flow curve for pure Ag nanopaste (0 wt% Cu), pure Cu nanopaste (100 wt% Cu) and Ag-Cu nanopaste with various Cu loadings (20-80 wt%)	139
Figure 4.18	XRD diffractogram for sintered pure Ag nanopaste (0 wt% Cu), sintered pure Cu nanopaste (100 wt% Cu) and sintered Ag-Cu nanopaste with various Cu loadings (20-80 wt% Cu) and for as-received raw Ag and Cu nanoparticles	141
Figure 4.19	Density and porosity error bar plot for sintered pure Ag nanopaste (0 wt% Cu), sintered pure Cu nanopaste (100 wt% Cu) and sintered Ag-Cu nanopaste with various Cu loadings (20-80 wt% Cu) (the spherical symbols in plot represent mean values)	143
Figure 4.20	FE-SEM micrographs for pure Ag nanopaste (0 wt% Cu), pure Cu nanopaste (100 wt% Cu) and Ag-Cu nanopaste with various Cu loadings (20-80 wt%) that sintered at temperature of 380 °C and open air ambient	145

Figure 4.21	AFM micrographs for pure Ag nanopaste (0 wt% Cu), sintered Cu nanopaste (100 wt% Cu) and Ag-Cu nanopaste with various Cu loadings (20-80 wt%) that sintered at temperature of 380 °C and open air ambient	147
Figure 4.22	Mean grain size and surface roughness (RMS) for sintered pure Ag nanopaste (0 wt% Cu), sintered pure Cu nanopaste (100 wt% Cu) and sintered Ag-Cu nanopaste with various Cu loadings (20-80 wt%)	148
Figure 4.23	Electrical conductivity for sintered pure Ag nanopaste (0 wt% Cu), sintered pure Cu nanopaste (100 wt% Cu) and sintered Ag-Cu nanopaste with various Cu loadings (20-80 wt%) (the spherical symbols in the error bar represent mean values)	150
Figure 4.24	DSC curves for sintered pure Ag nanopaste (0 wt% Cu), sintered pure Cu nanopaste (100 wt% Cu) and Ag-Cu nanopaste with various Cu loadings (20-80 wt% Cu). Inset resolves the overlapped curves	154
Figure 4.25	Melting temperature of various die-attach systems and their operational temperature range	156
Figure 4.26	(a) DSC heat flow curves for empty pan baseline, Ag reference standard, sintered pure Ag nanopaste (0 wt% Cu), sintered pure Cu nanopaste (100 wt% Cu) and sintered Ag-Cu nanopaste with various Cu loadings (20-80 wt% Cu); (b) specific heat for sintered pure Ag nanopaste (0 wt% Cu), sintered Cu nanopaste (100 wt% Cu) and sintered Ag-Cu nanopaste with increasing of Cu loading (20-80 wt% Cu)	158
Figure 4.27	Thermal diffusivity for sintered pure Ag nanopaste (0 wt% Cu), sintered pure Cu nanopaste (100 wt% Cu) and sintered Ag-Cu nanopaste with increasing of Cu loading (20-80 wt% Cu) at temperature 25, 150 and 300 °C	159
Figure 4.28	Thermal conductivity for sintered pure Ag nanopaste (0 wt% Cu), sintered pure Cu nanopaste (100 wt% Cu) and sintered Ag-Cu nanopaste with increasing of Cu loading (20-80 wt% Cu) at temperature 25, 150 and 300 °C	161

Figure 4.29	(a) Thermal expansion as a function of temperature plot and (b) transition temperature of thermal expansion for sintered pure Ag nanopaste (0 wt% Cu), sintered pure Cu nanopaste (100 wt% Cu) and sintered Ag-Cu nanopaste with various Cu loadings (20-80 wt%)	166
Figure 4.30	Coefficient of thermal expansion (CTE) plot for sintered pure Ag nanopaste (0 wt% Cu), sintered pure Cu nanopaste (100 wt% Cu) and sintered Ag-Cu nanopaste with various Cu loadings (20-80 wt%)	167
Figure 4.31	Illustration of shrinkage of pore to accommodate the thermal expansion with rising temperature up to transition temperature (enlarges are the illustrations for the increment of inter-atomic distance with rising temperature)	169
Figure 4.32	Thermal conductivity plotted against CTE for various die-attach systems	172
Figure 4.33	Indentation hysteresis of sintered pure Ag nanopaste (0 wt% Cu), sintered pure Cu nanopaste (100 wt% Cu) and sintered Ag-Cu nanopaste with various Cu loadings (20-80 wt%)	178
Figure 4.34	Hardness of sintered pure Ag nanopaste (0 wt% Cu), sintered pure Cu nanopaste (100 wt% Cu) and sintered Ag-Cu nanopaste with various Cu loadings (20-80 wt%)	181
Figure 4.35	Stiffness of sintered pure Ag nanopaste (0 wt% Cu), sintered pure Cu nanopaste (100 wt% Cu) and sintered Ag-Cu nanopaste with various Cu loadings (20-80 wt%)	182
Figure 4.36	Young's modulus of sintered pure Ag nanopaste (0 wt% Cu), sintered pure Cu nanopaste (100 wt% Cu) and sintered Ag-Cu nanopaste with various Cu loadings (20-80 wt%)	183
Figure 4.37	(a) Lap shear stress-strain curve of strength of sintered pure Ag nanopaste (0 wt% Cu), sintered pure Cu nanopaste (100 wt% Cu) and sintered Ag-Cu nanopaste with various Cu loadings (20-80 wt%)	186

Figure 4.38	Bonding strength of sintered pure Ag nanopaste (0 wt% Cu), sintered pure Cu nanopaste (100 wt% Cu) and sintered Ag-Cu nanopaste with various Cu loadings (20-80 wt%)	187
Figure 4.39	Bonding strength of sintered Ag-20Cu nanopaste with various metallization layers on Cu substrate	194
Figure 4.40	FE-SEM shear surface micrographs for shear-off joint with various metallization layers on Cu substrate	195
Figure 4.41	FE-SEM cross sectional images for shear-off joint with various metallization layers on Cu substrate at a different magnification	196
Figure 4.42	FE-SEM cross sectional images for sintered nanopaste with 20 and 80 wt% of Cu loading attached on Au-coated Cu substrate at a different magnification	198
Figure 4.43	FE-SEM cross sectional images for Ag-coated SiC attached on either Ag-Ni or Au-Ni AlN DBC substrate using sintered Ag-20Cu nanopaste at different magnifications	200
Figure 4.44	FE-SEM cross sectional images for Au-coated SiC attached on either Ag-Ni or Au-Ni AlN DBC substrate using sintered Ag-20Cu nanopaste at different magnifications	201
Figure 4.45	FE-SEM cross sectional images for bare SiC attached on either Ag-Ni or Au-Ni AlN DBC substrate using sintered Ag-20Cu nanopaste at different magnifications	202

## LIST OF ABBREVIATIONS

ACA	:	Anisotropic conductive adhesive
AFM	:	Atomic force microscopy
CHNS	:	Carbon-hydrogen-nitrogen-sulfur
CTE	:	Coefficient of thermal expansion
DBC	:	Direct bonded copper
DI	:	De-ionized
DSC	:	Differential scanning calorimetry
EEE	:	Electrical and electronic equipment
EF-TEM	:	Energy-filtered transmission electron microscopy
EG	:	Ethylene glycol
FE-SEM	:	Field-emission scanning electron microscopy
ICA	:	Isotropic conductive adhesive
ICSD	:	Inorganic crystal structure database
IMC	:	Intermetallic compound
MEA	:	More electric aircraft
MEMS	:	Micro-electro-mechanical system
MOS	:	Metal-oxide-semiconductor
MW	:	Molecular weight
PWC	:	Printed wiring board
RMS	:	Root-mean-square
RoHS	:	Restriction of hazardous substance
TGA	:	Thermo-gravimetric analysis
TMA	:	Thermo-mechanical analysis

UV-Vis : Ultraviolet-visible spectroscopy

WEEE : Waste of electrical and electronic equipment

XRD : X-ray diffraction

## LIST OF SYMBOLS

$\alpha$	:	Coefficient of thermal expansion
$\beta$	:	Shape constant for a Berkovich indentation tip
$\varepsilon$	:	Buildup strain
$\rho$	:	Bulk density
$\rho_T$	:	Theoretical density
$\lambda$	:	Thermal diffusivity
$A$	:	Contact area
$C_{p1}$	:	Specific heat of the sintered nanopaste sample
$C_{p2}$	:	Specific heat of the reference standard
$E$	:	Young's modulus
$E_i$	:	Young's modulus of the Berkovich indentation tip
$E_r$	:	Reduced Young's modulus for sintered nanopaste
$H$	:	Hardness
$h$	:	Indentation depth
$h_c$	:	penetration contact depth
$h_{max}$	:	Maximum indentation depth of the sintered nanopaste by an indenter
$k$	:	Thermal conductivity
$\Delta L$	:	Change of the sample length
$L_o$	:	Original sample length
$M$	:	Performance index, the ratio of $K/\alpha$
$m_1$	:	Mass of the sintered nanopaste sample
$m_2$	:	Mass of the reference standard
$P$	:	Applied load

$P_{max}$	:	Maximum applied load by an indenter
$Q$	:	Heat flow per unit area
$S$	:	Stiffness
$T$	:	Temperature
$\Delta T$	:	Change of the temperature
$T_h$	:	Homologue temperature ratio
$T_m$	:	Melting temperature
$T_o$	:	Safety operational temperature
$\nu$	:	Poisson's ratio of sintered nanopaste
$\nu_i$	:	Poisson's ratio of the Berkovich indentation tip
$W_d$	:	Dry weight of sintered nanopaste sample
$W_s$	:	Weight of sintered nanopaste sample upon suspended in water
$W_w$	:	Weight of sintered nanopaste sample upon removed from water
wt%	:	Weight percent
$x$	:	Heat flow direction from die to substrate
$y_1$	:	Net heat flow of the sintered nanopaste sample
$y_2$	:	Net heat flow of the reference standard



## LIST OF PUBLICATIONS

### International Peer-Reviewed Journals (ISI Indexed):

1. K. S. Tan and K. Y. Cheong, “Advances of Ag, Cu, and Ag-Cu Alloy Nanoparticles Synthesized via Chemical Reduction Route”, *Journal of Nanoparticle Research*, vol. 15, pp. 1-29, 2013.
2. K. S. Tan and K. Y. Cheong, “Physical and Electrical Characteristics of Silver-Copper Nanopaste as Alternative Die-Attach”, *IEEE Transactions on Components, Packaging and Manufacturing Technology*, vol. 4, pp. 8-15, 2014.
3. K. S. Tan, Y. H. Wong and K. Y. Cheong, “Thermal Characteristic of Sintered Ag–Cu Nanopaste for High-Temperature Die-Attach Application”, *International Journal of Thermal Sciences*, vol. 87, pp. 169-177, 2015.
4. K. S. Tan and K. Y. Cheong, “Mechanical Properties of Sintered Ag–Cu Die-Attach Nanopaste for Application on SiC Device”, *Materials and Design*, vol. 64, pp. 166-176, 2014.

### **International Conference Proceedings:**

1. K. S. Tan and K. Y. Cheong, “Effect of Sintering Temperature on Silver-Copper Nanopaste as High Temperature Die Attach Material”, *2<sup>nd</sup> International Conference on Sustainable Materials Engineering (ICoSM)*, Bayview Beach Resort, Penang, Malaysia, 26<sup>th</sup>-27<sup>th</sup> March 2013.
2. V. R. Manikam, K. S. Tan, K. A. Razak and K. Y. Cheong, “Nanoindentation of Porous Die Attach Materials as a Means of Determining Mechanical Attributes”, *3<sup>rd</sup> International Conference on Advances in Mechanical Engineering*, Hotel Equatorial, Melaka, Malaysia, 28<sup>th</sup>-29<sup>th</sup> August 2013.
3. K. S. Tan and K. Y. Cheong, “Effect of Sintering Environment on Silver-Copper Die-Attach Nanopaste”, *36<sup>th</sup> International Electronics Manufacturing Technology Conference (IEMT)*, Renaissance Johor Bahru Hotel, Johor, Malaysia. 11<sup>th</sup>-13<sup>th</sup> November 2014.

# **KAJIAN TERHADAP NANO-PES ARGENTUM-KUPRUM SEBAGAI BAHAN LAMPIR-DAI UNTUK APLIKASI SUHU TINGGI**

## **ABSTRAK**

Satu nano-pes argentum-kuprum (Ag-Cu) yang dirumuskan dengan mencampurkan nanopartikel Ag dan Cu dengan penambah organik (pelekat resin, terpineol dan ethylene glycol) telah dihasilkan bagi diaplikasikan sebagai bahan lampir-dai suhu tinggi. Pelbagai peratus berat nanopartikel Cu (20-80 wt%) telah ditambahkan ke dalam nano-pes Ag-Cu, diikuti oleh pensinteran di udara terbuka pada suhu 380 °C selama 30 min tanpa bantuan tekanan luar, untuk mengkaji kesan terhadap sifat-sifat fizikal, elektrik, terma dan mekanikal. Nanopes tulen Ag dan Cu turut disediakan untuk tujuan perbandingan. Keputusan belauan sinar-X menunjukkan fasa  $\text{Ag}_{97}\text{Cu}_3$ ,  $\text{Ag}_1\text{Cu}_{99}$  dan CuO terbentuk dalam nano-pes Ag-Cu tersinter. Kajian menunjukkan bahawa keliangan didalam nano-pes Ag-Cu tersinter meningkat dengan peningkatan kandungan Cu. Kehadiran keliangan tersebut membuktikan kesannya untuk mengurangkan ketumpatan, saiz bijian, keberaliran elektrik, keberaliran haba dan pekali pengembangan haba (CTE) bagi nano-pes Ag-Cu tersinter. Walaupun keliangan turut menjejaskan kekerasan, kekukuhan dan modulus Young nano-pes Ag-Cu tersinter, namun aliran meningkat telah direkodkan dengan penambahan kandungan Cu. Secara keseluruhan, nano-pes Ag-Cu dengan kandungan 20 wt% Cu menunjukkan kombinasi terbaik bagi keberaliran elektrik [ $2.27 \times 10^5 (\Omega\text{-cm})^{-1}$ ] dan haba [159 W/m-K]. Nilai-nilai tersebut didapati lebih tinggi daripada kebanyakan sistem bahan lampir-dai. CTE yang rendah [ $13 \times 10^{-6} / \text{K}$ ] yang berkait dengan nano-pes Ag-Cu tersebut memanfaatkan disebabkan ia mengelakkan pembentukan tekanan haba serius di antara dai dan substrat. Selain itu,

nano-pes Ag-Cu telah menunjukkan suhu lebur 955 °C, yang membolehkan nano-pes Ag-Cu dapat dipertimbangkan untuk diaplikasikan pada suhu tinggi. Bagi kajian sifat ikatan terhadap persalutan logam, salutan Ag and Au pada substrat Cu masing-masing telah menunjukkan kekuatan ikatan tertinggi (52.6 MPa) dan terendah (34.4 MPa) bagi nano-pes Ag-Cu. Nilai kekuatan ikatan didapati berkait rapat dengan mikrostruktur di antara nano-pes Ag-Cu dan lapisan salutan logam pada substrat. Akhir sekali, untuk mengaplikasikan nanopes Ag-Cu sebagai bahan lampir-dai pada suhu tinggi, nano-pes Ag-Cu telah digunakan untuk melampirkan dai silikon karbida (SiC) pada substrat yang disaluti oleh Ag atau Au. Keseluruhan struktur ikatan tersebut telah lulus ujian penuaan haba pada 770 °C, mikrostruktur yang telah mengalami proses penuaan haba menunjukkan bahawa nano-pes Ag-Cu merekat dengan baik pada dai SiC dan substrat yang disaluti Ag. Namun, perekatan nano-pes tersebut adalah kurang memuaskan pada dai SiC dan substrat yang disaluti Au.

# **INVESTIGATIONS ON SILVER-COPPER NANOPASTE AS DIE-ATTACH MATERIAL FOR HIGH TEMPERATURE APPLICATIONS**

## **ABSTRACT**

A silver-copper (Ag-Cu) nanopaste formulated by mixing Ag and Cu nanoparticles with organic additives (i.e., resin binder, terpineol and ethylene glycol) which is meant for high-temperature die-attach applications has been developed. Various weight percent of Cu nanoparticles (20-80 wt%) has been loaded into the Ag-Cu nanopaste, followed by sintering in open air at temperature of 380 °C for 30 min without the need of applied external pressure. The physical, electrical, thermal and mechanical properties were investigated. Both pure Ag and Cu nanopastes were also prepared for comparison purposes. X-ray diffraction results showed that  $\text{Ag}_{97}\text{Cu}_3$ ,  $\text{Ag}_1\text{Cu}_{99}$ , and CuO phases were formed in sintered Ag-Cu nanopaste. Studies revealed that the porosity of sintered Ag-Cu nanopaste increased with an increase of Cu loading, where the presence of porosity has shown its effect in decreasing of density, grain size, electrical conductivity, thermal conductivity and coefficient of thermal expansion (CTE). Although the porosity has also affected the hardness, stiffness and Young's modulus of sintered Ag-Cu nanopaste, yet an increasing trend has been recorded for aforementioned properties, with the increment of Cu loading. Overall, Ag-Cu nanopaste with 20 wt% of Cu loading has offered the best combination of electrical [ $2.27 \times 10^5 (\Omega\text{-cm})^{-1}$ ] and thermal conductivity [159 W/m-K], where these values are higher than most of the die-attach systems. The low CTE [ $13 \times 10^{-6}/\text{K}$ ] that associated with Ag-Cu nanopaste was good to prevent severe buildup of thermal stress between die and substrate. The Ag-Cu nanopaste has demonstrated a melting temperature of 955 °C, which enables it to be

considered for high-temperature applications. For metallization and bonding attribute studies, Ag and Au coatings on Cu substrate have displayed the highest (52.6 MPa) and the lowest (34.4 MPa) bonding strength for Ag-Cu nanopaste, respectively. The values of bonding strength were found to have a close relationship with the interface microstructure between Ag-Cu nanopaste and metallization layer on the substrate. Finally, to realize Ag-Cu nanopaste as a high-temperature die-attach material, the Ag-Cu nanopaste was used to attach a silicon carbide (SiC) die on a substrate with either Ag or Au coating. The entire bonding structure has passed a three-cycle thermal aging test at 770 °C. The thermal-aged interface microstructure has shown that the Ag-Cu nanopaste was well adherence to SiC die and substrate with Ag coating, but poor adherence to SiC die and substrate with Au coating.

## CHAPTER 1

### INTRODUCTION

#### 1.1 Theoretical background

The demand of electronic devices that could be operated at high-temperature ( $> 500\text{ }^{\circ}\text{C}$ ) is continually increasing for years. This is mainly due to the advancement of technology in various industries such as automotive, aviation, well-logging, nuclear power plant and space exploration. These industries require electronic devices that must not only be able to survive upon expose to high-temperature, but they must also be able to function under such high-temperature condition. For instance, the typical high-temperature applications for those industries are: (i) brake and exhaust gas sensors for automotive ( $300\text{-}1000\text{ }^{\circ}\text{C}$ ) (Johnson *et al.*, 2004; Spetz *et al.*, 1999), (ii) turbine and gas sensors for aviation ( $\sim 600\text{ }^{\circ}\text{C}$ ) (Dreike *et al.*, 1994; Hunter *et al.*, 2004; Sharp, 1999b), (iii) geothermal sensor for well-logging ( $\sim 600\text{ }^{\circ}\text{C}$ ) (Neudeck *et al.*, 2002; Sharp, 1999b; Watson and Castro, 2012), (iv) nuclear radiation detector and nuclear reactor for nuclear plant ( $700\text{-}1000\text{ }^{\circ}\text{C}$ ) (Dreike *et al.*, 1994; Kim *et al.*, 2011; Sedlackova *et al.*, 2013), and (v) transmitter, antenna and electromechanical devices for space exploration ( $> 500\text{ }^{\circ}\text{C}$ ) (Sutton, 2001). For such demanding applications, there is an evolution of electronic device, which transforming from silicon (Si)-based to silicon carbide (SiC)-based, due to the former could only operate at temperature up to  $250\text{ }^{\circ}\text{C}$ .

SiC-based electronic device has documented its success to operate at a temperature exceeding  $500\text{ }^{\circ}\text{C}$ . This is mainly attributed to the wide band gap

semiconductor properties (3.26 eV) and high breakdown field strength (3.2 MV/cm) that associated with SiC semiconductor. These properties allow SiC semiconductor to be operated at high-temperature without leakage of current (Chin *et al.*, 2010). Nevertheless, to take full advantages of SiC-based electronic device, there is a need to develop an electronic packaging, which can use for high-temperature applications. The main development areas of electronic packaging include die-attach material, substrate material, wire bonding material, and encapsulation material. Of these, die-attach material has gained particular concern as it is an integral part that provides connection between the SiC device and the substrate.

Ideally, a die-attach material for SiC device should demonstrate a melting temperature that is higher than 500 °C, which allows it to be operated in a high-temperature environment. It should also demonstrate a low processing temperature, as well as ease to be applied for mass production. Besides, another four main properties required are: electrical and thermal conductivities, coefficient of thermal expansion (CTE), and bonding strength. These properties must display values that are comparable to or superior than the benchmark requirements that listed in Table 1.1.

Table 1.1: Benchmark requirements of various die-attach properties for SiC device (Abtew and Selvaduray, 2000; Bai *et al.*, 2006b; Chin *et al.*, 2010; Chung, 1995; Haque *et al.*, 2012; Lu *et al.*, 2004; Manikam and Cheong, 2011).

Property	Benchmark requirement
Melting temperature	> 500 °C
Electrical conductivity	$\geq 0.71 \times 10^5 (\Omega \cdot \text{cm})^{-1}$
Thermal conductivity	$\geq 51 \text{ W/m-K}$



Table 1.1: Continued.

Property	Benchmark requirement
Bonding strength	$\geq 12.5$ MPa
Coefficient of thermal expansion	Close to the die and the substrate

## 1.2 Problem statement

Over the past decade, conductive adhesives (Gao *et al.*, 2014; Gomatam and Mittal, 2008; Lahokallio *et al.*, 2014; Li and Wong, 2006; Yim *et al.*, 2008) and tin (Sn)-based solders alloys (lead-bearing and lead-free) (Abtew and Selvaduray, 2000; Koo *et al.*, 2014; Kotadia *et al.*, 2014; Liu *et al.*, 2008; Wu *et al.*, 2004; Zeng *et al.*, 2012; Zeng and Tu, 2002; Zhang *et al.*, 2012) have been widely used for level-one interconnection, namely die-attach material, which serves to attach a semiconductor die on a substrate. The wide use of conductive adhesive and Sn based solder alloys are mainly due to the low cost and acceptable electrical conductivity [ $0.01\text{-}0.71 \times 10^5$  ( $\Omega\text{-cm}$ )<sup>-1</sup>] and thermal conductivity [ $1\text{-}66$  W/m-K] (Abtew and Selvaduray, 2000; Calame *et al.*, 2005; Gao *et al.*, 2014; Guan *et al.*, 2010; Kisiel and Szczepański, 2009; Kotadia *et al.*, 2014; Lewis and Coughlan, 2008; Navarro *et al.*, 2012; Suganuma *et al.*, 2009). However, with the recent development of SiC device that could be operated at temperature exceeding 500 °C (Manikam and Cheong, 2011), conductive adhesive and Sn based solder alloys that melt at a temperature below 315 °C (Abtew and Selvaduray, 2000; Kotadia *et al.*, 2014; Lahokallio *et al.*, 2014; Wu *et al.*, 2004; Zeng and Tu, 2002) can no longer meet the operating temperature requirement. The challenge is thus driven to seek a die-attach material that can be operated at temperature higher than 500 °C.

Bismuth (Bi) (Kim *et al.*, 2014; Shi *et al.*, 2010; Song *et al.*, 2007a; Song *et al.*, 2006; Spinelli *et al.*, 2014; Wang *et al.*, 2014b), gold (Au) (Bazin *et al.*, 2014; Chidambaram *et al.*, 2012; Ding *et al.*, 2013; Huang *et al.*, 2013; Lau *et al.*, 2013; Zhu *et al.*, 2014), and zinc (Zn) (Haque *et al.*, 2012; Haque *et al.*, 2010; Kim *et al.*, 2009a; Shimizu *et al.*, 1999) based solder alloys are next being proposed as alternative solutions. Of these, Bi based solder alloys have generally displayed poor electrical conductivity [ $0.02\text{-}0.12 \times 10^5 \text{ (}\Omega\text{-cm)}^{-1}$ ] (Kim *et al.*, 2014; Song *et al.*, 2007a; Song *et al.*, 2006), poor thermal conductivity [7-11 W/m-K] (Lalena *et al.*, 2002; Tschudin *et al.*, 2002) and moderate melting point [262-361 °C] (Lalena *et al.*, 2002; Spinelli *et al.*, 2014; Wang *et al.*, 2014b), which are inadequate to be considered as alternative solutions. Au and Zn based solder alloys, although, have displayed high thermal conductivity [27-110 W/m-K] (Bazin *et al.*, 2014; Kim *et al.*, 2009a; Kisiel and Szczepański, 2009; Suganuma *et al.*, 2009), their electrical conductivity [ $0.34\text{-}0.65 \times 10^5 \text{ (}\Omega\text{-cm)}^{-1}$ ] (Bazin *et al.*, 2014; Lau *et al.*, 2013) and melting point [280-383 °C] (Bazin *et al.*, 2014; Kim *et al.*, 2008; Kim *et al.*, 2009c; Lau *et al.*, 2013; Lee *et al.*, 2005; Sheen *et al.*, 2002; Weng *et al.*, 2013) are still lower than the benchmark values (Table 1.1), making them failed to be considered as suitable die-attach materials for SiC device. Au-nickel (Ni), with its high melting point of 980 °C, is an exceptional solder alloy that meets the operating temperature requirement ( $> 500 \text{ }^\circ\text{C}$ ) of SiC device, but its high soldering temperature at 980 °C has also become a drawback (Kirschman, 1999). Two new die-attachment techniques, namely inter-diffusion bonding of metal film and sintering of metal paste, are subsequently being introduced to overcome the weakness (i.e., high soldering temperature) that is associated with Au-Ni solder alloy. For instance, Au-indium (In) (Mustain *et al.*, 2010; Welch and Najafi, 2008) and silver (Ag)-In

(Chuang and Lee, 2002; Mustain *et al.*, 2010; Wu and Lee, 2013) are particular die-attach materials that utilized inter-diffusion bonding technique to form a joint between metal films at temperature of 206 to 210 °C with pressure of 40 to 80 psi. Meanwhile, Ag micropaste (Zhang and Lu, 2002) (i.e., a mixture of micro-sized metal particles and organic additives) and copper (Cu) micropaste (Kahler *et al.*, 2012b) are particular die-attach materials that formed a joint by sintering the micropaste at temperature of 250 °C with pressure of 40 MPa. Overall, the advantage of these die-attachment techniques is able to process at a moderate temperature (206-250 °C), yet the joint formed could be operated at temperature exceeds 495 °C (Kahler *et al.*, 2012b; Mustain *et al.*, 2010; Welch and Najafi, 2008; Wu and Lee, 2013; Zhang and Lu, 2002). On the other hand, application of pressure during the process is one of the disadvantages of these die-attachment techniques, which could complicate the manufacturing process and with slight irregularities during application of pressure may lead to cracking of both the die and the substrate (Kahler *et al.*, 2012b; Mustain *et al.*, 2010; Welch and Najafi, 2008; Wu and Lee, 2013; Zhang and Lu, 2002).

In recent years, a strategy of reducing the size of metal particle in metal paste, from micron to nano, has been introduced, which it is named as nanopaste (i.e., a mixture of nano-sized metal particles and organic additives). The reduction of particle size aims to increase the chemical driving force of metal particle and thus contributes to eliminate the application of pressure during sintering. Ag nanopaste (Bai *et al.*, 2007a; Bai *et al.*, 2007b; Bai *et al.*, 2005; Bai *et al.*, 2006b; Chen *et al.*, 2008; Lu *et al.*, 2014; Lu *et al.*, 2009; Mei *et al.*, 2011b, 2011c; Yu *et al.*, 2009; Zheng *et al.*, 2014) and Cu nanopaste (Krishnan *et al.*, 2012; Nishikawa *et al.*, 2011;

Yamakawa *et al.*, 2013) are the leading candidates of this strategy, where they could be sintered at temperature of 280-400 °C without the need of applying any pressure during sintering. Positive results were obtained for these sintered nanopastes, namely: (i) no existent of die-shifting issue as the nanopaste does not undergo liquid-state transformation during sintering (Bai *et al.*, 2007a; Bai *et al.*, 2007b; Krishnan *et al.*, 2012); (ii) high electrical [ $2.50\text{-}2.60 \times 10^5 \text{ } (\Omega\text{-cm})^{-1}$ ] and thermal conductivity [200-240 W/m-K] (Bai *et al.*, 2005; Bai *et al.*, 2006b; Lu *et al.*, 2004; Mei *et al.*, 2012; Zheng *et al.*, 2014); (iii) high bonding strength [2-54 MPa] could be attained with atomic inter-diffusion between the nanopaste and the metallization layer on a die or substrate (Bai *et al.*, 2007b; Nishikawa *et al.*, 2011; Yamakawa *et al.*, 2013); (iv) lower Young's modulus was detected for sintered nanopaste as compared to bulk materials and solder alloys; this is important to reduce the build-up of thermal stress among the die, die-attach and substrate in an operating device (Bai *et al.*, 2007b; Bai *et al.*, 2005; Bai *et al.*, 2006b; Mei *et al.*, 2012; Zheng *et al.*, 2014) and (v) high melting point at 960-1083 °C has meet the operating temperature requirement of a SiC device ( $> 500 \text{ } ^\circ\text{C}$ ) (Bai *et al.*, 2007b; Kahler *et al.*, 2012b; Lu *et al.*, 2004; Lu *et al.*, 2014; Mei *et al.*, 2011c; Zheng *et al.*, 2014). Despite that, both Ag nanopaste and Cu nanopaste are actually having their own limitations, where Ag nanopaste has limited to its high cost and low electrochemical migration resistance (Lu *et al.*, 2014; Mei *et al.*, 2011a); whereas Cu nanopaste is easy to oxidize. To overcome the oxidation issue, additional time (1h) is needed to anneal the Cu nanopaste in nitrogen environment (Krishnan *et al.*, 2012; Yamakawa *et al.*, 2013).

For these reasons, an Ag-aluminum (Al) nanopaste (Manikam *et al.*, 2012; Manikam *et al.*, 2013c) is introduced, which aimed at surpassing the preceding

limitations of Ag nanopaste and Cu nanopaste. This Ag-Al nanopaste not only could tailor the cost to be cheaper than that of Ag nanopaste, it also able to be sintered at 380 °C in air atmosphere without the need of additional annealing process in nitrogen environment. Ag-Al nanopaste has displayed electrical conductivity [ $1.01 \times 10^5 \text{ } (\Omega\text{-cm})^{-1}$ ] that is better than Sn, Bi, Au and Zn solder alloys [ $0.02\text{-}0.71 \times 10^5 \text{ } (\Omega\text{-cm})^{-1}$ ], but it is still worse than Cu micropaste [ $1.29 \times 10^5 \text{ } (\Omega\text{-cm})^{-1}$ ], Ag micropaste [ $4.17 \times 10^5 \text{ } (\Omega\text{-cm})^{-1}$ ] and Ag nanopaste [ $2.50\text{-}2.60 \times 10^5 \text{ } (\Omega\text{-cm})^{-1}$ ] (Bai *et al.*, 2005; Bai *et al.*, 2006b; Kahler *et al.*, 2012b; Manikam *et al.*, 2012; Zhang and Lu, 2002; Zheng *et al.*, 2014). Furthermore, Ag-Al nanopaste has also displayed thermal conductivity [123 W/m-K] that is better than Sn, Au, Bi and Zn solder alloys [7-110 W/m-K], but it is still worse than Ag micropaste [80-220 W/m-K] and Ag nanopaste [200-240 W/m-K] (Bai *et al.*, 2005; Bai *et al.*, 2006b; Kahler *et al.*, 2012b; Manikam *et al.*, 2012; Zhang and Lu, 2002; Zheng *et al.*, 2014).

Based on preceding facts, Ag-Cu nanopaste is introduced, which aimed to overcome the weakness that associated with Ag-Al nanopaste. Cu was chosen to replace Al in a nanopaste formulation because it has the second best electrical and thermal conductivities among other metals (Callister, 2007), and it has coefficient of thermal expansion that is comparable with Ag (Table 1.2), making it suitable to be used with Ag in a nanopaste formulation. Moreover, the price of Cu is comparable to that of Al ("Current pricing on precious, platinum, non ferrous, minor and rare earth metals," 2013), which is able to meet the cost constraint in electronic packaging. Although Cu and Al are ductile materials, Cu has higher tensile strength than Al (Table 1.2) (Callister, 2007), where higher bonding strength is predicted for Ag-Cu nanopaste if compared with Ag-Al nanopaste (Manikam *et al.*, 2013c;

Morisada *et al.*, 2010; Yan *et al.*, 2012). Based on galvanic series, Cu has standard electrode potential that is close to Ag if compared with Al to Ag, which minimize the tendency of two metals, i.e., Ag and Cu, to interact galvanically, and thus reduces the risk of galvanic corrosion (Chawla and Gupta, 1993). Ultimately, Cu has a melting temperature that is drastically higher than that of Al; this might make the melting temperature of Ag-Cu nanopaste become drastically higher than that of Ag-Al nanopaste.

Table 1.2: Properties of bulk Ag, Cu, Au and Al.

Property	Ag	Cu	Au	Al	Ref
Electrical conductivity [ $\times 10^5 (\Omega\text{-cm})^{-1}$ ]	6.80	6.00	4.30	3.80	(Callister, 2007)
Thermal conductivity [W/m-K]	428	398	315	247	(Callister, 2007)
Coefficient of thermal expansion [ $\times 10^{-6} / \text{K}$ ]	19.7	17.0	14.2	23.6	(Callister, 2007)
Tensile strength [MPa]	170	200	130	90	(Callister, 2007)
Young's modulus [GPa]	74	110	77	69	(Callister, 2007)
Ductility [% elongation]	44	45	45	40	(Callister, 2007)
Melting point [ $^{\circ}\text{C}$ ]	962	1085	1064	660	(Callister, 2007)
Price on March 2013 [\$ US / kg]	1012.36	7.61	56717.06	1.89	("Current pricing on precious, platinum, non ferrous, minor and rare earth metals," 2013)
Standard electrode potential [V]	+0.800	+0.340	+1.420	-1.662	(Callister, 2007)

In this work, the Ag-Cu nanopaste is formulated by mixing Ag and Cu nanoparticles with organic additives. This nanopaste can be sintered at 380 °C in open air without the need of applying external pressure. The study covered the detailed investigation of the physical, electrical, thermal and mechanical properties of Ag-Cu nanopaste with various Cu loadings, as these properties are crucial for die-attach applications. Further investigations were also carried out to assess the workability of Ag-Cu nanopaste as a die-attach material for SiC device, which is mainly for high-temperature applications.

### **1.3 Research objectives**

The primary aim of this research is to formulate an Ag-Cu nanopaste that can be used for high-temperature die-attach applications, yet it can be processed at a low-temperature. Various physical, electrical, thermal and mechanical properties of Ag-Cu nanopaste were systematically investigated, which include density, porosity, electrical conductivity, thermal conductivity, coefficient of thermal expansion, melting temperature, hardness, Young's modulus and bonding strength. These properties must be properly investigated in order to demonstrate the suitability of Ag-Cu nanopaste as a die-attach material for high-temperature applications (Table 1.1). With this primary aim in mind, the following objectives are to be achieved:

1. To formulate an Ag-Cu nanopaste by mixing metallic nanoparticle and organic additives, and determine its optimum sintering temperature and environment.

2. To investigate the physical, electrical and thermal characteristics of Ag-Cu nanopaste with various Cu loadings.
3. To investigate the mechanical properties of Ag-Cu nanopaste and its bonding attributes on different metallization layers.
4. To apply Ag-Cu nanopaste for attaching SiC die on Cu substrate and aluminium nitride direct bonded Cu substrate.

#### **1.4 Scope of study**

In this research work, Ag-Cu nanopaste was first formulated by mixing Ag and Cu nanoparticles with various loadings of organic additives. The rheology of nanopaste was next analyzed to determine an optimized formula for Ag-Cu nanopaste. Various sintering temperatures and environments were used to sinter the nanopaste which was aimed to obtain an optimized sintering condition. The research was next continued to investigate the physical, electrical, thermal and mechanical properties of Ag-Cu nanopaste with various weight percent of Cu loadings. The Ag-Cu nanopaste with optimized properties was selected for further investigation on its bonding attribute on different metallization coatings. Finally, the workability of Ag-Cu nanopaste as a high-temperature die-attach material has been investigated, where it was used to attach a SiC die on either Cu substrate or aluminium nitride direct bonded Cu substrate. The entire bonding structure has undergone a thermal aging test, followed by a cross-section failure analysis.

Various characterization techniques have been used in this work, where they are classified into physical, electrical, thermal and mechanical characterizations. For



physical characterization, rheometer was used to reveal the viscosity of nanopaste. Field emission scanning electron microscope (FE-SEM) and atomic force microscope (AFM) were used to characterize the surface morphology and topography of sintered Ag-Cu nanopaste. X-ray diffraction (XRD) was used to identify the phases, and co-linear four point probe system was used to measure the electrical conductivity of sintered nanopaste. For thermal characterization, differential scanning calorimetry (DSC) was used to determine the melting temperature of raw Ag and Cu nanoparticles. It also used to determine the melting temperature and specific heat of sintered Ag-Cu nanopaste. Besides, thermogravimetric analysis (TGA) was used to determine the burn off temperature of organic additives used in Ag-Cu nanopaste. The thermal diffusivity and thermal expansion attributes of sintered nanopaste were measured by using nanoflash laser and thermo-mechanical analysis (TMA) systems, respectively. As for mechanical characterization, nanoindentation technique was used to determine the hardness, stiffness and Young's modulus of sintered Ag-Cu nanopaste; whilst, lap shear test has been performed by using Instron universal testing machine to obtain the bonding strength of Ag-Cu nanopaste. The lap shear test was also performed on Cu substrate with various metallization coatings in order to understand the bonding attributes of Ag-Cu nanopaste.

## **1.5 Thesis outline**

This thesis is organized and divided into 5 chapters. Chapter 1 provides an overview of high-temperature electronic packaging, followed by the issues and challenges faced in the development of high-temperature die-attach

material, research objectives, and scope of study. Chapter 2 covers the detailed literature review, which corresponds to the background theories adopted in the study. Chapter 3 presents the systematic methodology that was employed in this research. Chapter 4 focuses on the results and discussion from the characterizations. Finally, Chapter 5 summarizes the overall findings of this study and concluded with appropriate recommendation for future works.

## CHAPTER 2

### LITERATURE REVIEW

#### 2.1 Introduction

In recent years, electronic devices are continually improving for high-temperature applications, mainly due to the increasing demand from various industries such as automotive, aviation, well-logging, nuclear power plant and space exploration (Chin *et al.*, 2010). These electronic devices are fabricated by using a wide band-gap semiconductor, namely silicon carbide (SiC), which aim at overcoming the limitation of low operating temperature ( $< 250\text{ }^{\circ}\text{C}$ ) that exhibited by conventional silicon (Si)-based electronic device (Chin *et al.*, 2010). The current research trend is thereby targeted to develop electronic packaging that is in line with the SiC-based electronic device, which is able to operate at high-temperature. This chapter begins by reviewing the evolution of electronic device from Si-based to SiC-based, followed by their applications. The chapter will next cover an overview of electronic packaging and the materials used for high-temperature applications. Since this research is focused on developing a die-attach material, the basic requirements of a die-attach material will be discussed. Next, the detailed literatures for high-temperature die-attach materials will be systematically covered. Finally, this chapter will review the factors affecting the mechanical, electrical, and thermal properties of die-attach material.

## **2.2 Definition of high-temperature for electronic device**

“High-temperature” is a term that subject to various interpretations, where it can be defined as a temperature that is greatly higher than a typical standard operating temperature (Chin *et al.*, 2010). For instance, automotive, well logging and space exploration industries have defined the term of “high-temperature” as an operating temperature at beyond 125 °C (Johnson *et al.*, 2004), 300 °C (Palmer and Heckman, 1978) and 500 °C (Hagler *et al.*, 2011), respectively. Hence, it is inadequate to define the term of “high-temperature” in accordance to respective industry. The definition must be determined from a group of variety industries, followed by taking into considerations the operating temperature of various electronic devices in the group. Manikam and Cheong (2011) are the leading researchers who proposed three ranges of temperature based on a group of variety industries. “High-temperature” is defined as a range of temperature that operates at beyond 500 °C; whilst, “medium-temperature” and “low-temperature” are defined as another ranges of temperature that operate at 300-500 °C and < 300 °C, respectively (Manikam and Cheong, 2011). In this thesis, these three ranges of temperature will be used; whereby “high-temperature” is fixed at a temperature that higher than 500 °C.

## **2.3 Evolution of semiconductor in electronic device**

Over the past decade, Si has emerged as the most widely used semiconductor materials in electronic devices. This is mainly due to its interesting attributes, such as (i) able to be produced in a large defect-free single crystal, (ii) able to grow a

stable native oxide layer ( $\text{SiO}_2$ ) that possesses superior dielectric properties, (iii) has appropriate hardness that allows large wafer can be handled by either hand or machine, (iv) able to be doped with small amount of impurities (e.g. phosphorus or boron), which formed either n-type or p-type semiconductor, and (v) relatively cheap in cost because of its relatively abundance in the earth crust (Chante *et al.*, 1998; Harper, 2003). However, with advances in technology for recent years, there is a demand of electronic devices that could be operated at high-temperature ( $\geq 500^\circ\text{C}$ ) and harsh environment. The electronic devices that based on Si semiconductor, with a maximum operating temperature of  $250^\circ\text{C}$ , have become no longer meet the requirement of high operating temperature. The low operating temperature ( $\leq 250^\circ\text{C}$ ) of Si semiconductor is actually attributed by its narrow band-gap (1.12 eV), in which leakage of electric current happens if it is operated at temperature beyond  $250^\circ\text{C}$  (Chante *et al.*, 1998). As a result, it is crucial to seek a semiconductor material that is capable to operate at temperature beyond  $250^\circ\text{C}$ .

In recent years, SiC semiconductor, with its large band-gap (3.26 eV), has identified as a promising candidate to overcome the limitation of Si semiconductor in an electronic device, due to its operating temperature is drastically improved to  $400^\circ\text{C}$  and above. Besides that, SiC semiconductor could also display a few advantages of Si semiconductor, such as (i) able to produce high quality single crystal with low defect, (ii) able to grow native oxide of  $\text{SiO}_2$ , and (iii) able to selectively dope of either n-type or p-type (Friedrichs and Rupp, 2005). These advantages are also contributing to make SiC becomes an interesting alternative semiconductor material for high-temperature applications. Table 2.1 provides a comparison of semiconductor properties between Si and SiC. It can be seen that the

SiC with large band-gap has offered a high breakdown electric field (3.2 MV/cm), which is approximately ten times higher than that of Si (0.3 MV/cm) with narrow band-gap. High breakdown electric field allows the SiC to be operated at a high-temperature without leakage of current if compared to Si. The thermal conductivity of SiC (3.7 W/cm-K) is approximately two times higher than that of Si (1.5 W/cm-K); this is good for heat dissipation in an operating electronic device.

Table 2.1: A comparison of semiconductor properties between Si and SiC  
(Chelnokov and Syrkin, 1997; Chin *et al.*, 2010; Zolper, 1998).

Property	Si	SiC
Band-gap (eV)	1.12	3.26
Dielectric constant	11.80	9.66
Breakdown electric field (MV/cm)	0.3	3.2
Thermal conductivity (W/cm-K)	1.5	3.7
Saturated electron velocity (cm/s)	$1 \times 10^7$	$2 \times 10^7$
Electron mobility ( $\text{cm}^2/\text{Vs}$ )	1400	1000
Hole mobility ( $\text{cm}^2/\text{Vs}$ )	600	115
Melting point ( °C)	1417	2827
Physical stability	Good	Excellent
Process maturity	Very high	High

In addition, the saturated electron velocity of SiC ( $2 \times 10^7$  cm/s) is also two times higher than that of Si ( $1 \times 10^7$  cm/s); this indicates that SiC can be operated at much faster speed if compared to Si. A SiC semiconductor is actually made up of Si and C atoms that held by a strong bond. The Si-C bond, in fact, is stronger than Si-Si bond that contains within a Si semiconductor. This strong bond provides better physical and chemical stabilities over the SiC semiconductor, which allows it to be operated in a high-temperature and harsh environment (Chin *et al.*, 2010).

### **2.3.1 Demands of high-temperature electronic device**

Nowadays, consumer electronic products, such as personal computer, cell phone, television and washing machine, have become an integral part in our daily lives. These products are commonly made up of Si-based electronic device, where it is continuously strike to decrease its feature size, increase its operating speed, and reduce its power consumption. Normally, the consumer electronic products are designed to be operated at temperature below 200 °C; thereby Si-based electronic device is sufficient to meet the requirements of those products.

On the other hand, the demands of industrial electronic components, such as radiation and pressure sensors, are slightly varied to those consumer electronic products. The industries are seeking for electronic components that are capable to be operated at high-temperature, high-power and harsh environment. The Si-based electronic device, with its low operating temperature ( $< 250\text{ }^{\circ}\text{C}$ ), is therefore no longer fulfill the requirements of industry electronic components. SiC-based electronic device, with its high operating temperature ( $> 400\text{ }^{\circ}\text{C}$ ), is next emerging as a promising candidate to overcome the limitations of conventional Si-based electronic device. For instance, the hydrocarbon sensor that made up of SiC has proven able to operate at temperature up to about 800 °C (Shields, 1996).

Over the years, the demand of high-temperature electronic devices has shown a steady growth due to the continuous technology advances in various industries. Oil and gas industry, in particular, is one of the leading industries that have high demand on the high-temperature electronic devices. This industry requires

a lot of fairly sophisticated sensors that to be installed in vicinity to the drilling head (Chin *et al.*, 2010). During a well drilling operation, the sensors are used to monitor the health of drilling head, as well as, used to measure the drilling depth as a function of temperature. This is due to the temperature variation in earth crust, which can be ranging up to 600 °C for the deepest drilling depth that can be attained by current drilling technology (Chin *et al.*, 2010; Sharp, 1999b). For well logging process (down-hole measurement), the sensors are used to acquire the down-hole information, such as surrounding geologic formation and saturation of hydrocarbon (oil and gas) (Watson and Castro, 2012). This information is important to determine the amount of hydrocarbon that can be extracted from the well. Finally, during the hydrocarbon extraction process, the sensors and electronic systems are used to monitor the pressure, temperature, vibration, and flow rate of hydrocarbon; this is to ensure an optimized productivity from the well, while also prevents any catastrophic disaster (Chin *et al.*, 2010; Sharp, 1999b; Watson and Castro, 2012).

Aviation is another industry that requires a large volume of high-temperature electronic devices, which arise from the main goal that moving towards the “more electric aircraft” (MEA) (Reinhardt and Marciniak, 1996; Santini *et al.*, 2013; Watson and Castro, 2012). Traditional commercial aircraft is operated with a centralized control system, which involved large amounts of complex wiring, piping and connector interfaces to transmit the signal and power from the central electronic controller to the mechanical, hydraulic and pneumatic systems that located in an aircraft (Santini *et al.*, 2013). In line with the target of MEA, distributed control system is being introduced to replace the centralized control system in an aircraft, where the electronic controllers are placed near to the engines (Watson and Castro,



2012). This system offers five main advantages: (i) it reduces the complexity of wiring interconnections, thereby reducing the maintenance complexity and cost; (ii) it reduces the amount of long and heavy wiring and piping systems, thereby saving the weight of an aircraft; (iii) it increases the control reliability because of a number reduction in connector pins; (iv) it increases the survivability of an aircraft since malfunction of certain electronic controllers still can allow an aircraft landing safely; and (v) it provides better fuel efficiency and increases performance of an aircraft (Reinhardt and Marciniak, 1996; Watson and Castro, 2012). The trade off, however, is the electronic controller needs to be operated at high-temperature environment that is close proximity to the engine. For instance, the electronic controller that monitors rotational speed of turbine disk in an aircraft engine, it has to withstand an elevated temperature up to 600 °C (Nieberding and Powell, 1982). Another example is the electronic controller and sensor that used for combustion emission monitoring; they need to operate to the temperature ranging up to 800 °C (Hunter *et al.*, 2004; Sharp, 1999b).

The automotive industry is a fairly substantial market, which requires large quantities of high-temperature electronic devices. This is due to the evolution of the automotive industry that is transforming from mechanical and hydraulic systems to an electromechanical system (Huque *et al.*, 2008). The evolution is mainly aimed to improve fuel efficiency and reduce emissions of an automobile. Consequently, more sensors and signal-conditioning components are being installed into an automobile in order to precisely control the valve timing (Chin *et al.*, 2010; Sharp, 1999a). Nowadays, an advanced automobile contains approximately 100 sensors, where these sensors are used to monitor the health of engine, angular position and speed,

automatic brake system, power steering, and exhaust system (Fleming, 2001; Sharp, 1999a). Those sensors are being installed in various locations of an automobile, in which the operating temperature is also varied according to the install locations, as shown in Table 2.2. For instance, the sensors for automatic braking and exhaust systems are working under an ambient temperature of 300 °C and 1000 °C, respectively (Sharp, 1999a; Spetz *et al.*, 1999).

Table 2.2: Automotive maximum operating temperatures (Johnson *et al.*, 2004; Spetz *et al.*, 1999).

Sensors install locations	Maximum operating temperature ( °C)
On-engine	150-200
In-transmission	150-200
On wheel-automatic brake system	150-300
Cylinder pressure	200-300
Exhaust system	Up to 1000

Space exploration is a niche market of electronic devices, but its operating temperature and environment is rather high and harsh. Starting from the launch of the space shuttle, the sensors are used to monitor the combustion of hydrocarbon at a temperature up to 1000 °C and above, as well as, used to detect any leakage of hydrocarbon (Sutton, 2001). This is to ensure a safe journey from the earth to the outer space. For Venus planet exploration, the surface temperature of this planet is ranging between 460 °C and 480 °C, with a surface pressure of 92 bars, carbon dioxide and nitrogen atmospheres, and sulfuric acid cloud coverage at a distance of 50 km from the surface (Cressler and Mantoot, 2013). The electronic devices that have landed on this planet must be able to withstand those harsh conditions first, followed by executing the given missions on this planet.

On the other hand, high-temperature electronic devices are also being used in other industrial applications, including nuclear power plant and industrial production machine. The nuclear power plant utilized a lot of sophisticated sensors that are made up of SiC semiconductor. These sensors are being used wisely to detect the neutron formation and its liberated radiation at a temperature of 700 °C (Kim *et al.*, 2011; Sedlackova *et al.*, 2013). Besides, the sensors are also being installed in surrounding the storage tanks of nuclear waste, which function to detect any leakage of radioactive and hazardous substances, at a temperature of up to perhaps 150 °C (Dreike *et al.*, 1994). All of these applications could be beneficial to prevent any possibility of catastrophic disaster happens to the nearby citizens. For industrial production applications, such as ammonia production plant, the sensor is being used to monitor the synthesized concentration of ammonia, where it must able to withstand a high temperature, up to 500 °C, that to be applied in the production process (Timmer *et al.*, 2005). Other industrial applications include temperature, pressure, flame indicator, and ultraviolet radiation sensors, which operate at a medium- to high-temperature, ranging between 450 °C and 1050 °C (Casady and Johnson, 1996; Shields, 1996). In summary, the applications of high-temperature electronic device are a large variety in accordance with the industrial requirements. Although the market of industrial electronic components is not as large as consumer electronic products, but its market has steadily grown in recent years, and therefore the market cannot be ignored too.

## **2.4 An overview of electronic packaging**

High-temperature electronic device has been realized with the development of SiC semiconductor technology. Nevertheless, the electronic device cannot be worked without a proper packaging. Therefore, the packaging, or more specifically termed as electronic packaging, must be developed in order to connect the electronic device to other components of electronic package, namely substrate, heat sink, printed wiring board and power source (Tummala, 2001). Figure 2.1 illustrates a three-level hierarchy of electronic packaging. At first-level of electronic packaging, also known as device level packaging, an electronic device or chip is to be connected to a package that serves as protecting, powering and cooling mediums. This level of packaging also functions to provide signal transmission from a chip to the package, or vice versa, where electrical conductive pads on both the chip and the package are to be connected via wire bonding. The first-level electronic package is next interconnected to a second-level electronic package, which is typically a printed wiring board (PWB). It is because a single device or chip does not generally form into a system, as a typical system requires a number of different types of active and passive devices that to be assembled and interconnected via a printed wiring board. The motherboard is next used to connect several pieces of printed wiring boards and functions to provide an integration of entire system; this is typically referred to as third-level of electronic packaging (Tummala, 2001).

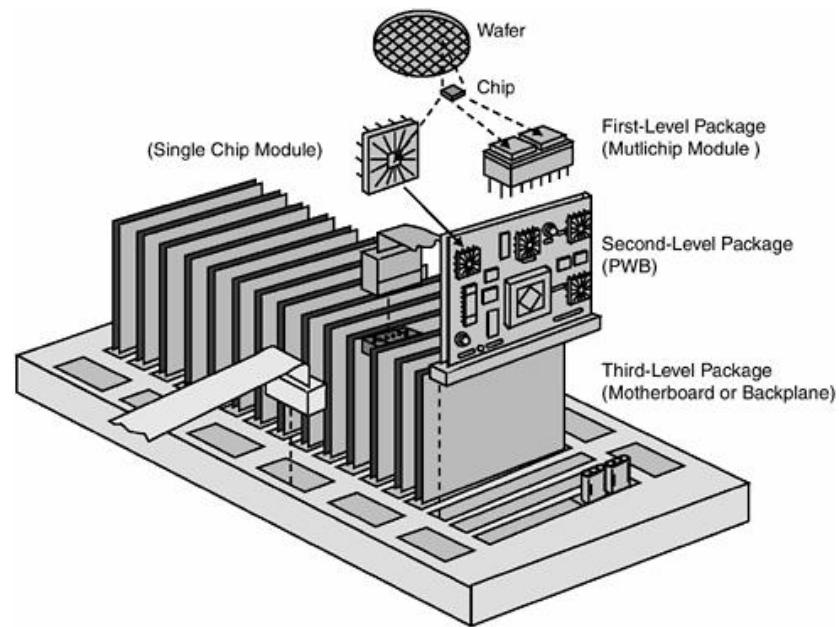


Figure 2.1: Hierarchy of electronic packaging (Tummala, 2001).

## 2.5 Materials for level-one electronic packaging

Currently, the development of high-temperature electronic device has focused on two broad areas, which are semiconductor device fabrication and its packaging. A substantial research effort has been spent on the development of electronic device that based on SiC semiconductor which aims for high-temperature applications. This is owned to its intrinsic wide band gap semiconductor with excellent physical and mechanical properties. Various electronic devices have been successfully produced by SiC semiconductor, such as the metal-oxide-semiconductor (MOS) field effect device that is designed for gas sensor applications (Soo *et al.*, 2010). The SiC-based sensor has displayed a high sensitivity and selectivity for sensing a variety of gases, namely hydrogen, oxygen, and hydrocarbon. Table 2.3 provides a summary of various gases that can be sensed by

current SiC-based gas sensors, in which the operating temperature of those sensors can be ranged up to 1000 °C.

Table 2.3: A summary of various gases sensed by SiC-based gas sensors.

Gas sensed by SiC sensor	Maximum operating temperature ( °C)	Reference
H <sub>2</sub>	150-800	(Ghosh and Tobias, 2005)
O <sub>2</sub>	300-800	(Ghosh and Tobias, 2005)
CO	650	(Baranzahi <i>et al.</i> , 1997)
H <sub>2</sub> S	325	(Weng <i>et al.</i> , 2008)
CH <sub>4</sub>	350	(Soo <i>et al.</i> , 2010)
C <sub>2</sub> H <sub>6</sub>	650	(Baranzahi <i>et al.</i> , 1995)
C <sub>3</sub> H <sub>6</sub>	350-700	(Kandasamy <i>et al.</i> , 2005)
C <sub>4</sub> H <sub>10</sub>	650	(Baranzahi <i>et al.</i> , 1995)
C <sub>x</sub> H <sub>y</sub>	500-1000	(Werner and Fahrner, 2001)

Although the SiC-based electronic devices, such as gas sensors, have been well designed for high-temperature applications, but these devices cannot be worked without a proper electronic packaging that acts to transmit the signal from a device to other computerized systems, as well as, to provide a protection for the device in against of its surrounding harsh environments (Kirschman, 1999). For device level packaging (level-one of electronic packaging), there are four main areas need to be concerned for high-temperature applications, namely die-attach material, substrate material, wire bonding material, and encapsulation material. These electronic packaging materials must be properly designed, where their properties must also be properly addressed in fulfillment of the requirements for high-temperature applications. In this thesis, the primary focus is on die-attach material that serves to attach an electronic device or die on a substrate. The die-attach material is actually an integral part of electronic package, as it acts as an interface layer between a die